Fractional-order impulse response of the respiratory system

Clara Ionescu, Jose Tenreiro Machado, Robin De Keyser

A B S T R A C T

This paper presents the measurement, frequency-response modeling and identification, and the corresponding impulse time response of the human respiratory impedance and admittance. The investigated adult patient groups were healthy, diagnosed with chronic obstructive pulmonary disease and kyphoscoliosis, respectively. The investigated children patient groups were healthy, diagnosed with asthma and cystic fibrosis, respectively. Fractional order (FO) models are identified on the measured impedance to quantify the respiratory mechanical properties. Two methods are presented for obtaining and simulating the time-domain impulse response from FO models of the respiratory admittance: (i) the classical pole-zero interpolation proposed by Oustaloup in the early 90s, and (ii) the inverse discrete Fourier Transform (DFT). The results of the identified FO models for the respiratory admittance are presented by means of their average values for each group of patients. Consequently, the impulse time response calculated from the frequency response of the averaged FO models is given by means of the two methods mentioned above. Our results indicate that both methods provide similar impulse response data. However, we suggest that the inverse DFT is a more suitable alternative to the high order transfer functions obtained using the classical Oustaloup filter. Additionally, a power law model is fitted on the impulse response data, emphasizing the intrinsic fractal dynamics of the respiratory system.

Keywords:
Respiratory mechanics
Fractional order
Frequency response
Impulse response
Fourier Transform
Admittance

1. Introduction

A recent trend has been observed in the signal processing community to introduce the concept of fractional order modeling in biological systems [1,2]. Initial characterizations of the lung's mechanical properties have been reported in invasive animal studies, showing the necessity of a fractional order (FO) integral in characterizing the viscoelastic properties of the lung mechanics based on analogy to a rubber balloon [3–6]. Several studies show that dynamic systems with recurrent geometry comprise phenomena which describe the specific material/system with recurrent mechanical properties as well [7–9]. Model performance analysis has shown that an FO model outperforms an integer-order model for characterizing frequency-dependence in human respiratory input impedance [10,11]. The advantage of FO models over the integer order models is their low number of parameters. An FO model can be implemented with integer-order approximations, but in a limited frequency range and requiring high orders [8]. The disadvantage of such approximations in clinical practice is their difficult interpretation and high number of parameters to be related to lung pathology. Our previous observations demonstrated that in case of input impedance models, both integral and differential FO must be present [11,12]; while for transfer impedance models in animal studies it is sufficient to have an FO integral to characterize the mechanical properties of lung tissue [3,4].

Table 1
Biometric and spirometric parameters of the investigated adults subjects. Values are presented as mean ± standard deviation; % pred: predicted according to the asymptomatic males of the present study; VC: vital capacity; FEV_1: forced expiratory volume in one second. H_A — healthy; KS_A — kyphoscoliosis; $COPD_A$ — chronic obstructive pulmonary disease. *n* denotes the number of tested volunteers.

ADULTS	H_A $n = 42$	KS_A $n = 24$	$COPD_A$ $n = 39$
Age (years)	27 ± 2	62 ± 10	64 ± 3
Height (m)	1.73 ± 0.27	1.55 ± 0.08	1.73 ± 0.14
Weight (kg)	69 ± 5.6	63 ± 15	79 ± 12
VC % (pred)	–	33 ± 14	84 ± 12
FEV_1 % (pred)	–	31 ± 11	38 ± 6

Table 2
Biometric and spirometric parameters of the investigated children subjects. Values are presented as mean ± standard deviation; % pred: predicted according to the asymptomatic males of the present study; VC: vital capacity; FEV_1: forced expiratory volume in one second; *FEF*: forced expiratory flow; H_C — healthy; A_C — asthma; CF_C — cystic fibrosis. *n* denotes the number of tested volunteers.

CHILDREN	H_C $n = 33$	A_C $n = 44$	CF_C $n = 38$
Age (years)	9 ± 1	11 ± 4	14 ± 6
Height (m)	1.35 ± 0.05	1.40 ± 0.2	1.49 ± 0.15
Weight (kg)	32 ± 6	36 ± 15	40 ± 11
FEF/VC % (pred)	–	85 ± 31	86 ± 9
FEV_1/VC % (pred)	–	97 ± 1.2	95 ± 0.9

In this paper, the determination of the impulse response from the frequency response of the respiratory admittance is presented by means of two algorithms: (i) the Oustaloup filter and (ii) the inverse discrete Fourier transform (DFT). The frequency response is available from fractional order models identified on measured impedance in six groups of subjects: three groups of adults and three groups of children.

Bearing these facts in mind, the paper is organized as follows: the next section introduces the patient database and the measurement protocol, along with the modeling techniques used to obtain the respiratory impedance and admittance. The two methods for obtaining the time-domain dynamics from the frequency response of a system are briefly explained: the Oustaloup filter and the inverse DFT. The results are presented in the third section, followed by a short discussion. The main outcome of this investigation is summarized in a conclusion section and points to some research ideas.

2. Materials and methods

2.1. Patients

There are six sets of data collected from subjects which are available for our analysis. These are both children, as well as adult subjects, for health and respiratory disorders. The biometric and spirometric details are given in Tables 1 and 2 for adults and children, respectively. As a general remark, it should be noted that each specific group was tested in a single location and that both the team and the device employed to perform the lung function tests was always the same.

These subjects have been initially diagnosed based on lung function tests performed during forced inspirations and forced expirations by means of a spirometer [13]. In combination with other physiological measurements, the vital capacity (VC) can help making a diagnosis of the underlying lung disease. Vital capacity is the maximum amount of air a person can expel from the lungs after a maximum inspiration. VC is equal to the inspiratory reserve volume plus the tidal volume plus the expiratory reserve volume. Force vital capacity (FVC) is the maximum volume of air that a person can exhale after maximum inhalation. FVC can also be the maximum volume of air that a person can inhale after maximum exhalation. Another important measure during spirometry is the forced expired volume in one second (FEV_1). The FEV_1/FVC ratio is used in the diagnosis of *obstructive* and *restrictive* lung disease, and normal values are approximately 80% [13]. In obstructive lung disease, the FEV_1 is reduced due to obstruction to air escape. Thus, the FEV_1/FVC ratio will be reduced. In restrictive lung disease, the FEV_1 and FVC are equally reduced due to fibrosis or other lung pathology (not obstructive pathology). Thus, the FEV_1/FVC ratio should be approximately normal. Factors that cause abnormal compliance are those which destroy the lung tissue, causing it to become fibrotic or edematous, blocks the bronchioli or hinders lung expansion and contraction. When considering the compliance of the lungs and thorax together, one should keep in mind any abnormality of the thoracic cage (e.g., kyphosis, scoliosis) [14].

In all measurements, drop-out criteria were: (i) technically biased measurements (swallowing, coughing, glottis closure); (ii) fatigue and therefore reduced ability to breath spontaneously; and (iii) irregular breathing period. All subjects and patients were in stable physical conditions at the time of the evaluation.

Written and/or oral consent was obtained from all participants, and in case of children, from both children and their parents. Further selection of the participants was performed by oral/written questionnaire ruling out any other respiratory

disease than the one envisaged for the study at the time of measurement or in the four weeks prior to the test. The results presented in this paper are obtained only from the data to whom these inclusion criteria applied.

2.1.1. Measurements in adults

The **healthy adult group** (H_A) evaluated in this study consists of 42 Caucasian volunteers (students) without a history of respiratory disease, whose lung function tests were performed in our laboratory.[1] Table 1 presents their biometric parameters and the measured impedance data was validated using prediction values [15], based on their height, weight, age and gender. The identified values from our measurements remained close to the predicted values and within the 95% confidence interval.

Chronic Obstructive Pulmonary Disease in adults ($COPD_A$) denotes any disorder that persistently obstructs the bronchial airflow [16]. However, it mainly involves two related diseases: chronic bronchitis and emphysema. Both cause chronic obstruction of air flowing through the airways and in and out of the lungs. The obstruction is irreversible and progresses (becomes worse) over time. The $COPD_A$ group under study consisted of 39 Caucasian COPD-diagnosed patients under observation at the "Leon Danielo" Hospital in Cluj-Napoca, Romania. The patients were former coal miners from the Petrosani area in Romania. Their biometric and spirometric parameters are given in Table 1.

Kyphoscoliosis in adults (KS_A) is a disease of the vertebrae, mostly beginning in childhood [14]. The deformation of the spine characteristically consists of a lateral displacement or curvature (scoliosis) or an antero-posterior angulation (kyphosis) or both (kyphoscoliosis). The angle of the spinal curvature called *the angle of Cobb* determines the degree of the deformity and consequently the severity of the restriction. The study on the KS_A group was approved by the local Ethics Committee of the University Hospital Gent-Belgium and informed consent was obtained from all volunteers before inclusion in the study. It involved 24 data sets from adults diagnosed with significant kyphoscoliosis (Cobb angle$=75°$) and their corresponding biometric and spirometric values are given in Table 1.

2.1.2. Measurements in children

The measurements on the 33 **healthy children** (H_C) were performed at the St. Vincentius Basis School in Zwijnaarde, Belgium; the biometric details are given in Table 2. The children had no history of pulmonary disease, and were selected using a specific questionnaire. The questionnaire verified the absence of dyspnoea, chronic cough, wheeze in the chest, etc. The measurements performed on healthy children have been verified with predicted values [17], based on their height. All measured data was validated within the 95% confidence interval values.

Asthma in children (A_C) denotes a pulmonary disease in which there is obstruction to the flow of air out of the lungs, but the obstruction is usually reversible and, between attacks of asthma, the flow of air through the airways is usually good [18]. In an asthma attack, the muscles in the airways contract (bronchospasm), causing narrowing of the airway walls. Asthma can be controlled using specific medication (inhaled steroids). The data for this study was recorded at the University Hospital Antwerp-Belgium, from 44 asthmatic children data sets whose corresponding biometric and spirometric values are given in Table 2.

Cystic fibrosis in children (CF_C) is one of the most common severe (genetic) diseases, characterized by the production of abnormal secretions, leading to mucous build-up and persistent inflammation in a variety of organs [19,20]. The data used in this study was recorded at the University Hospital Antwerp from 38 data sets from children diagnosed with cystic fibrosis whose biometric and spirometric values are given in Table 2.

2.2. Measuring the respiratory impedance

The impedance was measured using the Forced Oscillation Technique (FOT) standard setup, commercially available, assessing respiratory mechanics from 4 to 48 Hz in steps of 2 Hz. The subject is connected to the typical setup from Fig. 1 via a mouthpiece, suitably designed to avoid flow leakage at the mouth and dental resistance artifact. The oscillation pressure in most recent FOT devices is generated by a loudspeaker (LS) connected to a chamber, namely the SPH-165KEP MONACOR, with a range from 3–1000 Hz. The LS is driven by a power amplifier fed with the oscillating signal generated by a computer, namely a HP Pavilion dv1000 with a Pentium M processor, 1.5 GHz, 512 MB with 266 MHz SDRAM. The movement of the LS cone generates a pressure oscillation inside the chamber, which is applied to the patient's respiratory system by means of a flexible respiratory tube of 1 m length and 2 cm diameter, connecting the LS chamber and the bacterial filter (bf). A side opening (BT) of the main tubing allows the patient to decrease total dead space re-breathing (i.e. 40 ml). This bias tube exhibits high impedance at the excitation frequencies to avoid the loss of power from the LS pressure chamber [21]. During the measurements, the patient wears a nose clip and keeps the cheeks firmly supported to reduce the artifact of upper airway shunt. Pressure and flow are measured at the mouthpiece, respectively by means of (i) a pressure transducer (PT) and (ii) a pneumotachograph (PN) plus a differential pressure transducer (PT). The high precision pressure transducers are BSDX0050D4D, with a bipolar pressure range from 0 to 1 kPa, accuracy of 0.004 kPa and a common mode rejection ratio of 80 dB over the frequency range of interest. The working range is a peak-to-peak size between 0.1–0.3 kPa, in order to

[1] Ghent University, Belgium.

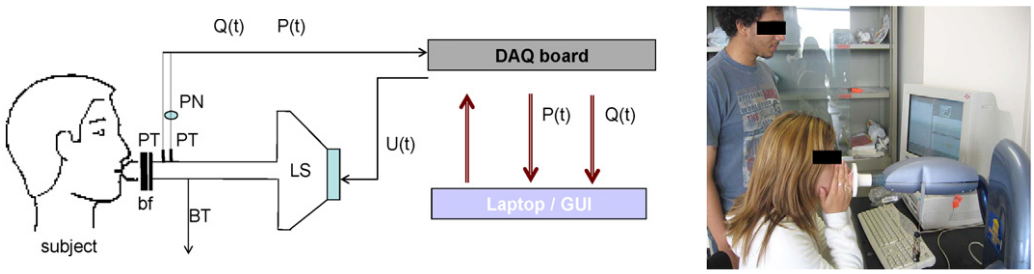

Fig. 1. A schematic overview and photo of the device with patient performing the FOT lung function test. Legend: LS — loudspeaker; BT — bias-tube; PN — pneumotachograph; PT — pressure transducer; bf — biological filter with mouthpiece; Q — flow; P — pressure; $U(t)$ — driving signal (test input).

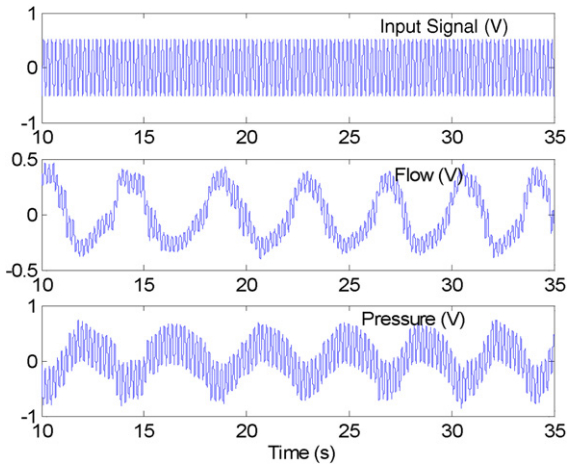

Fig. 2. Typical measured signals from one subject: oscillatory driving pressure; trans-respiratory pressure and air-flow. The breathing of the patient (low frequency) can be observed superimposed on the multisine signals.

ensure optimality, patient comfort and stay within a narrow range in order to assume linearity [22]. The flow is measured using a Hans Rudolph pneumotachograph, covering a range of 0–400 l/min, (6.6 l/s), 4830B series, with a dead space volume between 0–6.66 ml.

Averaged measurements from 3–5 technically acceptable tests should be taken into consideration for further signal processing. Exclusion criteria were: swallowing, coughing, irregular breathing pattern, or a coherence function below 0.8. The signals are acquired using a PCMCIA DAQ card 4026E series, 12bit from National Instruments, sampled every 1 ms. Typical time-records are depicted in Fig. 2.

All patients were tested in the sitting position, with cheeks firmly supported and elbows resting on the table. The posture is important in estimating values for respiratory impedance and, therefore a straight back was as much as possible applied (some patients who were too tall for the adjusted maximum height of the device, were excluded from the database). Each and every group of patients and volunteers has been tested in its unique location, using the same FOT device, and under the supervision of the same FOT team.

2.3. Identification methods

2.3.1. Non-parametric identification

One of the most common non-parametric representations of the impedance Z_r (kPa s/l) is obtained assuming a linear dependence between the breathing and superimposed oscillations at the mouth of the patient [23]. Based on the electrical analogy, pressure corresponds to voltage and flow corresponds to current. Hence, the respiratory impedance Z_r can be defined as the spectral (frequency domain) ratio:

$$Z_r(j\omega) = \frac{S_{PU(j\omega)}}{S_{QU(j\omega)}} \tag{1}$$

where $S_{ij}(j\omega)$ denotes the cross-correlation spectra between the various input–output signals, ω (rad/s) is the angular frequency and $j = \sqrt{-1}$, resulting in a complex variable evaluated in each frequency point of interest. The frequency where the imaginary part of the impedance crosses zero is called the *resonance frequency* and it depends on the balance between the different kind of mechanical properties (elastic, inertial). This then allows clinicians to visually classify between healthy

and pathologic cases, since the resonance frequency changes significantly with each respiratory disease. Further details are given in Appendix.

2.3.2. Parametric identification

In order to obtain a quantitative measure of respiratory mechanical properties, parametrization is employed. In [10,11], it was suggested that a model with two FO (one derivative, one integral) can give best results for the respiratory impedance evaluated in the interval $f \in [4, 48]$ Hz:

$$Z(j\omega) = L_r(j\omega)^{\alpha} + \frac{1}{C_r(j\omega)^{\beta}} \tag{2}$$

with $0 \leq \alpha \leq 1, 0 \leq \beta \leq 1$, C_r the compliance (l/kPa) and L_r the inductance (kPa s^2/l). Using the definition of complex numbers, (2) becomes:

$$Z(j\omega) = L_r\omega^{\alpha}\cos(\pi/2\alpha) + \frac{1}{C_r\omega^{\beta}}\cos(\pi/2\beta) + j\left[L_r\omega^{\alpha}\sin(\pi/2\alpha) - \frac{1}{C_r\omega^{\beta}}\sin(\pi/2\beta)\right]. \tag{3}$$

From the real and imaginary parts in (1), parametric identification has been employed and the models parameters were estimated using a nonlinear least squares optimization algorithm, making use of the MatLab® function `lsqnonlin`. The optimization algorithm is a subspace trust region method and is based on the interior–reflective Newton method described in [24]. The large-scale method for `lsqnonlin` requires that the number of equations (i.e., the number of elements of cost function) be at least as large as the number of variables. Every iteration involves the approximate solution using the method of preconditioned conjugate gradients, for lower and upper bounds. In this application, the lower bounds were set to 0 (parameters cannot have negative values) with no upper bounds. The optimization stopped either when a high number of iterations reached 100*nr. of variables, or a termination tolerance value of 10^{-8}. In all cases we obtained a correlation coefficient between data and model estimates above 80%. The solution is given as an optimal set of $(L_r, C_r, \alpha, \beta)$ parameters in (2). The model in (2) has been further employed to calculated the frequency response over a wide range of frequencies for the respiratory admittance:

$$Y(j\omega) = \frac{1}{Z(j\omega)}. \tag{4}$$

A student t-test was used to derive the 95% confidence intervals and ANOVA was used to compare model parameters among the measured groups. Results were considered significant at $p \leq 0.05$.

2.4. From frequency domain to time domain

2.4.1. Oustaloup filter

In the previous section, we have seen that a fractional order model of the impedance (2) can be fitted on the frequency-response (1) of the respiratory system in a given frequency band. However, this model cannot be used directly to simulate the time-response of the respiratory system (e.g. impulse response). A feasible solution is to use finite dimensional transfer functions of integer order. A good overview of such feasible implementations is given in [25]. From these methods, we shall adopt in this paper the classical method of pole-zero interpolation introduced by Oustaloup in early 1990s [26]. In the remainder of this paper, we shall refer to this method as the *Oustaloup filter*.

Oustaloup filter approximation to a fractional order differentiator is a widely used method in fractional calculus. A generalized Oustaloup filter defined in the frequency band $[\omega_b, \omega_h]$ can be represented as:

$$G(s) = K\prod_{k=1}^{N}\frac{s+p}{s+z} \tag{5}$$

with p poles, z zeros, K a gain, and N the number of pole-zero pairs (i.e. a design parameter). The poles, zeros and gain can be calculated from:

$$p = \omega_b \cdot \omega_u^{2k-1-\gamma/N} \tag{6}$$

$$z = \omega_b \cdot \omega_u^{2k-1+\gamma/N} \tag{7}$$

$$K = \omega_h^{\gamma} \tag{8}$$

with γ the fractional order of the derivative s^{γ} to be approximated and $\omega_u = \sqrt{\omega_h/\omega_b}$. The result will be an Nth integer order transfer function.

In this study, we have applied the approximation given by (5) for the s^{α} and the s^{β} coefficients from model (2). Consequently, the admittance becomes:

$$G(s) = \frac{g_2}{L_r \cdot g_1 \cdot g_2 + 1/C_r} \tag{9}$$

with g_1 and g_2 the approximations for s^{α} and s^{β}, respectively.

Table 3
Estimated and derived model parameters and modeling errors for all the investigated groups. Values are given as mean ± standard deviation; values in brackets indicate the corresponding 95% confidence intervals.

	L_r	$1/C_r$	α	β
H_A	0.032 ± 0.029	1.59 ± 1.10	0.42 ± 0.08	0.75 ± 0.11
	(0.019, 0.045)	(1.09, 2.08)	(0.38, 0.47)	(0.70, 0.80)
$COPD_A$	0.016 ± 0.007	2.81 ± 1.45	0.56 ± 0.07	0.52 ± 0.10
	(0.013, 0.019)	(2.15, 3.47)	(0.53, 0.60)	(0.47, 0.56)
KS_A	0.0173 ± 0.012	2.47 ± 0.76	0.54 ± 0.05	0.55 ± 0.05
	(0.007, 0.02)	(1.85, 3.10)	(0.49, 0.58)	(0.50, 0.59)
H_C	0.11 ± 0.08	4.73 ± 2.73	0.32 ± 0.11	0.63 ± 0.16
	(0.06, 0.15)	(3.2, 6.2)	(0.26, 0.38)	(0.54, 0.72)
A_C	0.13 ± 0.17	7.96 ± 3.16	0.32 ± 0.09	0.70 ± 0.13
	(0.03, 0.23)	(6.21, 9.7)	(0.27, 0.38)	(0.62, 0.77)
CF_C	0.07 ± 0.03	8.67 ± 4.63	0.38 ± 0.08	0.77 ± 0.15
	(0.05, 0.10)	(5.11, 12.23)	(0.31, 0.44)	(0.66, 0.89)

2.4.2. Inverse discrete Fourier transform IDFT

The Fourier transform of a signal $x(t)$ in time is used to obtain the frequency representation of that signal [27]:

$$\mathrm{FT}\{x\} = X(j\omega) = \int_{-\infty}^{\infty} x(t)\mathrm{e}^{-j\omega t}\mathrm{d}t \tag{10}$$

where $\omega = 2\pi f$ (rad/s) with f the frequency (Hz) and t is time (s). If we assume that x_k is a discrete sample of $x(t)$, we have the discrete Fourier transform (DFT):

$$\mathrm{DFT}\{x\} = \sum_{k=0}^{N-1} x_k \mathrm{e}^{-j\omega kT_s} \tag{11}$$

with k the sample number, T_s the sampling period and N the number of samples. Hence, the Fourier transform of a sequence of impulse functions, each of which is an element of the sample vector x, is equal to the DFT of x at each frequency where DFT is measured.

The inverse DFT is calculated as:

$$x(t) = \frac{1}{2\pi}\int_{-\infty}^{\infty} X(j\omega)\mathrm{e}^{j\omega t}\mathrm{d}\omega. \tag{12}$$

The result of (12) is the impulse response of the system whose frequency response is given by $X(j\omega)$.

2.5. Power law modeling

It has been shown that the respiratory system can be successfully modeled by recurrent ladder networks which preserve the morphology and the anatomy [10,9]. It was also shown that these ladder networks converge to a transfer function with fractional order operators [9,26]. Since the fractal dynamics can be well modeled by power law models (decay function), one may expect this property also from the respiratory system. We propose therefore to model the impulse response by the power law model:

$$x(t) = A \cdot t^B \tag{13}$$

with A and B identified constants using a similar nonlinear least squares algorithm as presented in Section 2.3.2 [24]. A student t-test was used to derive the 95% confidence intervals and ANOVA was used to compare model parameters among the groups. Results were considered significant at $p \leq 0.05$.

3. Results and discussion

The estimated model parameter for (2) are given in Table 3 for all subjects by means of mean and standard deviation values, along with 95% confidence intervals. These model parameters are then used to calculate the frequency response in a wide range of frequencies. Statistically significant differences were observed between the H_A, $COPD_A$ and KS_A groups ($p < 0.01$) and between H_C and A_C groups ($p < 0.01$). There were no significant differences between H_C and A_C groups, due to prior inhaled medication ($p < 0.29$) [28].

The tuning parameters for the Oustaloup filter were fitted in the frequency range 0–10^6 Hz, with 100 Hz frequency resolution, linearly spaced. The order of the filter set to $N = 20$ gave good results for all frequency responses. An illustrative example is given in Fig. 3 by means of the Bode plot, with the corresponding 22nd order transfer function in the form of (5) with the gain:

$$K = 245950.9486 \tag{14}$$

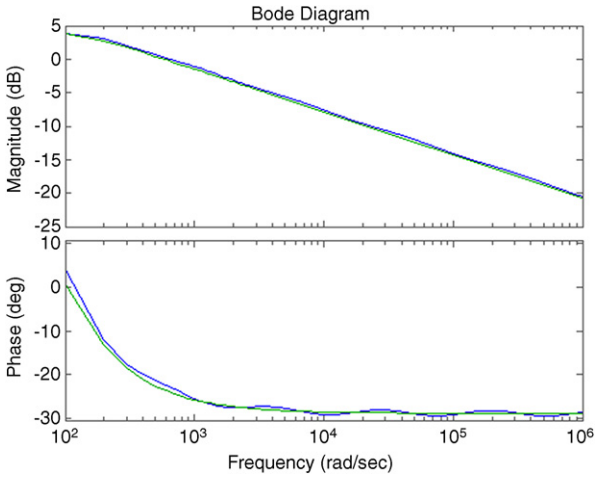

Fig. 3. An illustrative example of fitting the Oustaloup filter of order $N = 20$ to the frequency response of the respiratory admittance in one patient.

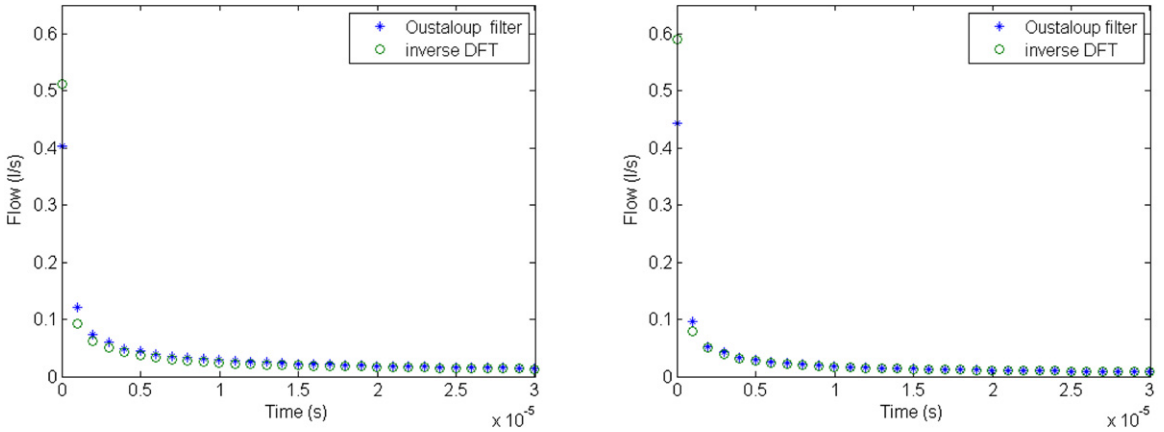

Fig. 4. Impulse responses for the adult healthy averaged data set (left) and for the healthy children averaged data set (right).

the denominator:

$$
\begin{aligned}
&s^4(s+4.759\cdot 10^{-8})(s+3.369\cdot 10^{-7})\\
&(s+2.385\cdot 10^{-6})(s+1.688\cdot 10^{-5})(s+0.0001195)(s+0.0008463)\\
&(s+0.005991)(s+0.04241)(s+0.3003)(s+2.126)(s+15.05)\\
&(s+106.5)(s+754.2)(s+5339)(s+37800)(s+2676\cdot 10^{-5})\\
&(s+1.895\cdot 10^{6})(s+1.111\cdot 10^{7})
\end{aligned}
\tag{15}
$$

and the numerator:

$$
\begin{aligned}
&s^2(s+2.645\cdot 10^{-8})(s+6.3\cdot 10^{-8})(s+1.873\cdot 10^{-7})\\
&(s+1.326\cdot 10^{-6})(s+9.386\cdot 10^{-6})(s+6.645\cdot 10^{-5})(s+0.0004704)\\
&(s+0.00333)(s+0.02358)(s+0.1669)(s+1.182)(s+8.366)\\
&(s+59.22)(s+419.3)(s+2968)(s+2.101\cdot 10^{4})\\
&(s+1.488\cdot 10^{5})(s+1.053\cdot 10^{6})\\
&(s+7.456\cdot 10^{6})(s+3.704\cdot 10^{7}).
\end{aligned}
\tag{16}
$$

For the inverse DFT method, the same frequency response as for the Oustaloup filter was used. The results from Fig. 4 show that the same type of impulse response is obtained with either method. Similar impulse responses are obtained for the other data sets. However, the Oustaloup filter is a high-order transfer function, containing coefficients which differ significantly in their magnitude. As such, the transfer function from (14)–(16) may not always pose numerical stability, since it contains

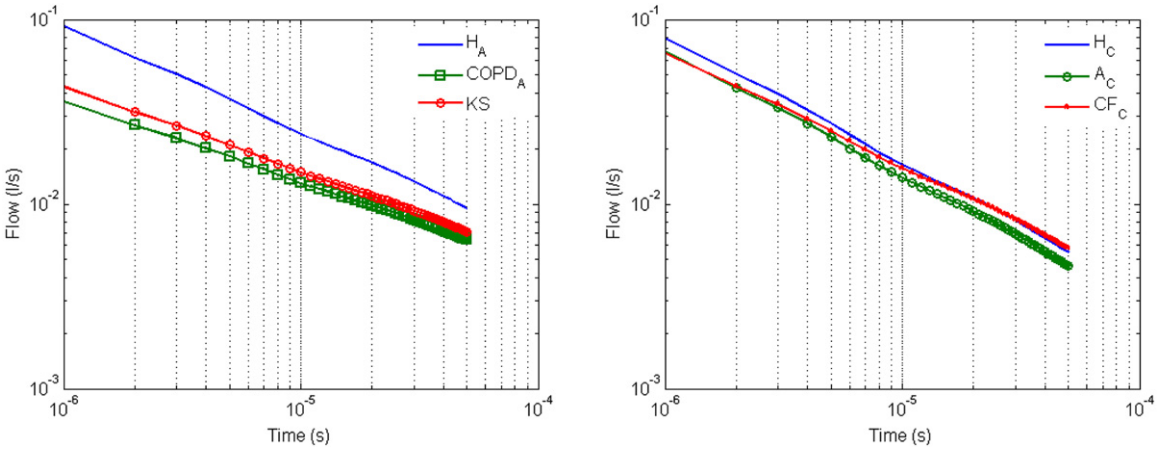

Fig. 5. Log–Log plot of the averaged impulse response of the admittance in adults (left) and in children (right).

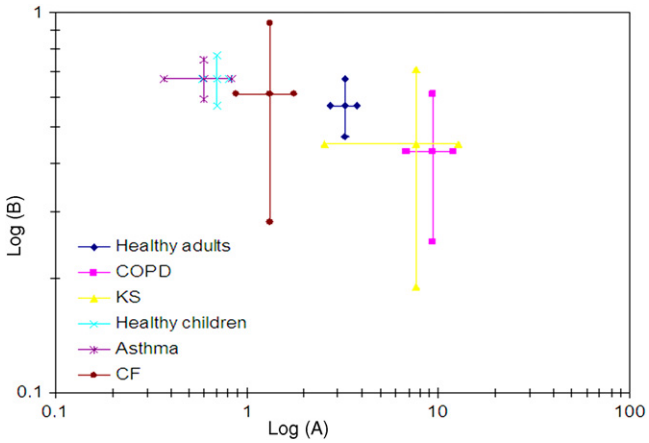

Fig. 6. The locus of the identified A and B values from model (13).

Table 4
Estimated power law model parameters (13) for all the investigated groups, from the corresponding impulse response. Values are given as mean ± standard deviation; values in brackets indicate the 95% confidence intervals.

	$A \cdot 10^{-5}$	$-B$	Res$\cdot 10^{-5}$
H_A	3.24 ± 0.51 (2.57, 4.93)	0.57 ± 0.10 (0.52, 0.61)	0.54 ± 0.16
$COPD_A$	9.43 ± 2.62 (7.65, 9.67)	0.43 ± 0.18 (0.39, 0.47)	0.05 ± 0.04
KS_A	7.68 ± 5.12 (7.05, 15.9)	0.45 ± 0.26 (0.41, 0.51)	0.09 ± 0.02
H_C	0.70 ± 0.11 (0.6, 0.9)	0.67 ± 0.10 (3.2, 6.2)	0.53 ± 0.15
A_C	0.60 ± 0.23 (0.40, 1.78)	0.67 ± 0.08 (0.61, 0.73)	0.38 ± 0.12
CF_C	1.33 ± 0.45 (1.08, 1.44)	0.61 ± 0.33 (0.55, 0.68)	0.30 ± 0.19

coefficients which vary broadly in magnitude $[10^{-8}, 10^{7}]$. The inverse DFT is numerically stable by definition and can serve to simulate the output of the respiratory system for any input signal.

Fig. 5 shows the log–log plots of the averaged values for impulse response in admittances for adults and for children groups, respectively. To the impulse response of each patient, a power law model as given by (13) has been identified and its values are given in Table 4. The locus plot of the values from Table 4 is depicted by Fig. 6.

From the results presented in this paper, it is clear that the specificity of the respiratory disorders in $COPD_A$ and KS_A respectively, has a significant impact on the fractal dynamics of the respiratory system ($p \ll 0.01$). However, the A_C group were controlled by means of medication, hence their lung function test was normal to the exam [28]. This is often the

case, since asthma does not manifest as a continuous phenomena, mostly being triggered by external factors (i.e. allergens). Bearing these facts in mind, it is no surprising that the fractal dynamics in H_C and in A_C are similar ($p < 0.2$). In CF_C, there is no specificity in the manifestation of the disease with respect to respiratory airways and tissue, but its manifestation is overall the respiratory airways and tissue ($p \ll 0.01$).

From a practical point of view, the impulse response describes the dynamics of the respiratory airways and tissue. The results depicted in Fig. 4 show that with disease, the amplitude is diminished and the decay is accelerated, showing viscous effect (i.e. fibrosis of the tissue). In other words, in patients suffering from obstructive ($COPD_A$, A_C) or restrictive disease (KS_A), a much higher pressure (impulse amplitude and time interval) must be applied to obtain the same air-flow as in the healthy. We can therefore conclude that the impulse response can serve as an evaluation tool for respiratory dynamics and mechanical properties.

4. Conclusions

This paper presented a real-life application where the fractional order models seem to be physically justified by the nature of the system to be modeled: the respiratory system. Data from healthy subjects and patients diagnosed with respiratory disease has been used to determine averaged model parameters in each group. The frequency response obtained from the fractional order model has been then used to determine the impulse response by means of two methods: (i) the pole-zero interpolation in the Oustaloup filter and (ii) the inverse discrete Fourier transform. The results show that both methods give similar impulse responses which can be further used for evaluating the dynamics of the respiratory airways and tissue. Additionally, a power law model fitted on the impulse response confirm the existence of intrinsic fractal dynamics.

Appendix. Physical interpretation of the respiratory impedance

For frequencies below 2 Hz, the respiratory system can be represented mechanically as a series connection of a resistance R and a compliance C. The driving pressure $P(t)$ generates flow $Q(t)$ across the resistance and the volume $V(t)$ changes in the compliance. If $P_r(t)$ and $P_e(t)$ are the resistive and elastic pressure drops respectively, we have that: $R = P_r(t)/Q(t)$; $C = V(t)/P_e(t)$ and $P(t) = P_e(t) + P_r(t)$. It results that:

$$P(t) = R \cdot Q(t) + V(t)/C. \tag{A.1}$$

This represents the first order equation in the motion-equation for a single compartment model of the respiratory system: a single balloon with compliance C on a pipeline with a resistance R. This system can be studied using the exponential decay of volume $V(t)$ as resulting from a step input V_0: $V(t) = V_0 e^{-t/\tau}$, where t is time and τ is the time constant which characterizes the system, denoted by the product of RC. However, in respiratory mechanics, the system is studied using a sinusoidal function at a given angular frequency ω. The pressure drop across the resistance is in phase with the flow, while the pressure across the elastic element is in phase with the volume. Using the exponential notation of sinusoidal functions, (A.1) can be re-written as function of flow:

$$P = R \cdot Q - j\frac{Q}{C\omega} \tag{A.2}$$

and division by Q results in the impedance formula: $P/Q = Z = R - j\frac{1}{C\omega}$. In this form, the resistance is the 'in-phase' component, while the compliance is the 'out-of-phase' component. The modulus is then defined by $|Z| = \sqrt{Re^2 + Im^2}$ with Re and Im denoting the real, respectively the imaginary part of the complex impedance. The phase is defined by $\Phi = \tan^{-1}(Im/Re) = \tan^{-1}(\frac{-1}{RC\omega}) = \tan^{-1}(\frac{-1}{\tau\omega})$.

When the pressure is oscillated at higher frequencies, an additional term, the inductance, must be introduced into the model to account for pressure changes in phase with the volume accelerations; resulting in the series R-L-C model structure. From electricity, we know that the potential difference over R, U_R, is in phase with the electrical current I in the circuit, while the potential over the inductance, U_L, leads the current by 90° and over the capacitance, U_C, lags it with 90°. We have that the total potential is given by: $U^2 = U_R^2 + (U_L - U_C)^2$. Since $U_R = I \cdot R$, $U_L = I \cdot X_L$, and $U_C = I \cdot X_C$ with X_L and X_C the resistance vectors of inductance and capacitance, it follows that $U = I\sqrt{R^2 + (X_L - X_C)^2}$.

The electrical impedance is given by $Z = \sqrt{R^2 + (X_L - X_C)^2}$ and $\tan\Phi = (X_L - X_C)/R$. Recalling that $X_L = L\omega$ and $X_C = 1/(\omega C)$ it follows that Z varies with the frequency of the applied potential difference of the alternating current. At a certain frequency, the so-called *resonance frequency*, $X_L - X_C = 0$, denoting the mechanical properties of the respiratory system. Depending on the inertial and compliant properties, the resonance frequency varies with healthy and pathologic lungs.

References

[1] A. Eke, P. Herman, L. Kocsis, L. Kozak, Fractal characterization of complexity in temporal physiological signals, Physiol. Meas. 23 (2002) R1–R38.
[2] B. West, Fractal physiology and the fractional calculus: a perspective, Front. Fractal Physiol. 1 (12) (2010) 1–17. Open source:www.frontiersin.org.
[3] Z. Hantos, B. Daroczy, B. Suki, S. Nagy, J. Fredberg, Input impedance and peripheral inhomogeneity of dog lungs, J. Appl. Physiol. 72 (1) (1992) 168–178.

[4] Z. Hantos, A. Adamicz, E. Govaerts, B. Daroczy, Mechanical impedances of lungs and chest wall in the cat, J. Appl. Physiol. 73 (2) (1992) 427–433.
[5] J. Hildebrandt, Comparison of mathematical models for cat lung and viscoelastic balloon derived by Laplace transform methods from pressure–volume data, Bull. Math. Biophys. 31 (1969) 651–667.
[6] J. Hildebrandt, Pressure–volume data of cat lung interpreted by a plastoelasitc, linear viscoelastic model, J. Appl. Physiol. 28 (1970) 365–372.
[7] K. Adolfsson, M. Enelund, P. Olsson, On the fractional order model of viscoelasticity, Mechanics of Time-dependent Materials 9 (2005) 15–34.
[8] A. Oustaloup, F. Levron, B. Mathieu, F. Nanot, Frequency-based complex noninteger differentiator: characterization and synthesis, IEEE Trans. Circuits Syst.- Part I 47 (2000) 25–39.
[9] C. Ionescu, I. Muntean, J.T. Machado, R. De Keyser, M. Abrudean, A theoretical study on modelling the respiratory tract with ladder networks by means of intrinsic fractal geometry, IEEE Trans. Biomed. Eng. 57 (2) (2010) 246–253.
[10] C. Ionescu, P. Segers, R. De Keyser, Mechanical properties of the respiratory system derived from morphologic insight, IEEE Trans. Biomed. Eng. 56 (4) (2009) 949–959.
[11] C. Ionescu, R. De Keyser, K. Desager, E. Derom, Fractional-Order Models for Characterizing the Impedance of the Respiratory System, G. Naik (Ed.), chapter 9 in book: Advances in Biomedical Engineering, pp. 377–396, ISBN 978-953-307-004-9, www.intechweb.org/books.php (open access), 2009.
[12] C. Ionescu, R. De Keyser, Parametric models for characterizing respiratory input impedance, Taylor and Francis J. Med. Eng. and Tech. 32 (4) (2008) 315–324.
[13] R. Northrop, Non-invasive Instrumentation and Measurement in Medical Diagnosis, CRC Press, 2002.
[14] F. McCool, D. Rochester, Non-muscular diseases of the chest wall, in: A. Fishman (Ed.), Fishman's Pulmonary Disease and Disorders, vol. II, McGraw Hall Medical, NY, 2008, pp. 1541–1548.
[15] H.G. Pasker, R. Schepers, J. Clment, K.P. Van de Woestijne, Total respiratory impedance measured by means of the forced oscillation technique in subjects with and without respiratory complaints, Eur. Resp. J. 9 (1996) 131–139.
[16] P.J. Barnes, Chronic obstructive pulmonary disease, NEJM Medical Progress 343 (2) (2000) 269–280.
[17] E. Duiverman, J. Clement, K. Van de Woestijne, H. Neijens, A. van den Bergh, K. Kerrebijn, Forced oscillation technique: reference values for resistance and reactance over a frequency spectrum of 2–26 Hz in healthy children aged 2.3–12.5 years, Clinical Resp. Physiol. 21 (1985) 171–178.
[18] W. Busse, R. Lemanske, Asthma, New Engl. J. Med. 344 (5) (2001) 350–362.
[19] S. Brennan, G. Hall, F. Horak, A. Moeller, P. Pitrez, A. Franzamann, S. Turner, N. de Clerck, P. Franklin, K. Winfield, E. Balding, S. Stick, P. Sly, Correlation of forced oscillation technique in preschool children with cystic fibrosis with pulmonary inflammation, Thorax 60 (2005) 159–163.
[20] A. Elizur, C. Cannon, T. Ferkol, Airway inflammation in cystic fibrosis, Chest 133 (2) (2008) 489–495.
[21] M. Birch, D. MacLeod, M. Levine, An analogue instrument for the measurement of respiratory impedance using the forced oscillation technique, Phys. Meas. 22 (2001) 323–339.
[22] E. Oostveen, D. Macleod, H. Lorino, R. Farré, Z. Hantos, K. Desager, F. Marchal, The forced oscillation technique in clinical practice: methodology, recommendations and future developments, Eur. Respir. J. 22 (2003) 1026–1041.
[23] B. Daröczy, Z. Hantos, An improved forced oscillatory estimation of respiratory impedance, Int. J. Bio-Medical Comput. 13 (1982) 221–235.
[24] T.F. Coleman, Y. Li, An interior trust region approach for nonlinear minimization subject to bounds, SIAM J. Optim. 6 (1996) 418–445.
[25] A. Monje, Y. Chen, B. Vinagre, D. Xue, V. Feliu, Fractional Order Systems and Controls, Springer-Verlag, 2010.
[26] A. Oustaloup, La dérivation Non-Entiere, Hermes, Paris, 1995.
[27] S. Stearns, Digital Signal Processing with Examples in Matlab, CRC Press, Boca Raton, 2003.
[28] C. Ionescu, K. Desager, R. De Keyser, Fractional order model parameters for the respiratory input impedance in healthy and in asthmatic children, Computer Methods Programs Biomedicine 101 (2011) 315–323.